

## Article

# Experimental Study of Frame-Supported Shear Wall Structure of High-Rise Buildings with Transfer Slab in Metro Depot

Yishu Xia <sup>1,2</sup>, Wuxiong Li <sup>3</sup>, Weiya Liu <sup>2</sup>, Yanhui Liu <sup>1,\*</sup>, Xin Xu <sup>1</sup> and Chenyun Zhang <sup>4</sup><sup>1</sup> Earthquake Engineering Research & Test Center (EERTC), Guangzhou University, Guangzhou 510006, China<sup>2</sup> Shenzhen Classical Building Structure Design Firm Co., Ltd., Shenzhen 518057, China<sup>3</sup> Shenzhen Metro Group Co., Ltd., Shenzhen 518026, China<sup>4</sup> Guiyang Vocational and Technical College, Guiyang 550023, China

\* Correspondence: liuyanhui@gzhu.edu.cn

**Abstract:** Taking the frame-supported shear wall structure of a 102.1 m high metro depot as the test object, the structure has obvious vertical irregularity, and a quasi-static test was carried out on the structural model with the scale of 1/5. The damage development and strain of the structure were observed by applying displacement loads under different seismic actions, and the experimental phenomena and measured data were analyzed. The results show that the safety performance of the structure meets the seismic requirements of the MCE (Maximum considered earthquake) condition. Under the action of load, a reasonable damage mechanism is formed in which the components above the transfer story crack first and those below the transfer story crack later, which is in line with the design concept of “the performance objective of the bottom frame structure is higher than that of the upper shear wall structure”. The transfer plate is mainly subjected to shear deformation, the possible shear failure of the transfer plate should be avoided by reasonable design. Due to the large height difference between the first floor and the second floor, the structure may be adversely affected, so it is necessary to make the yielding floor appear in the bottom strengthening part above the transfer story. Under the SLE (Service level earthquake) and DBE (Design based earthquake) conditions, the bottom frame of the structure is mainly subjected to elastic deformation. Under the MCE (Maximum considered earthquake) condition, the bottom frame of the structure causes a lot of damage, increases energy consumption and decreases stiffness, which further proves that “the performance goal of the bottom frame structure is higher than that of the upper shear wall structure”.

**Keywords:** frame-supported shear wall structure; transfer slab; vertical irregularity; soft-story; pseudo-static test; seismic performance



**Citation:** Xia, Y.; Li, W.; Liu, W.; Liu, Y.; Xu, X.; Zhang, C. Experimental Study of Frame-Supported Shear Wall Structure of High-Rise Buildings with Transfer Slab in Metro Depot. *Buildings* **2022**, *12*, 1940. <https://doi.org/10.3390/buildings12111940>

Academic Editor: André R. Barbosa

Received: 13 October 2022

Accepted: 9 November 2022

Published: 10 November 2022

**Publisher's Note:** MDPI stays neutral with regard to jurisdictional claims in published maps and institutional affiliations.



**Copyright:** © 2022 by the authors. Licensee MDPI, Basel, Switzerland. This article is an open access article distributed under the terms and conditions of the Creative Commons Attribution (CC BY) license (<https://creativecommons.org/licenses/by/4.0/>).

## 1. Introduction

With the acceleration of urbanization, land resources in densely populated cities are increasingly scarce, the study of transit-oriented development (TOD) has received attention and the application of multi-purpose high-rise building has been promoted. Transfer structural systems are widely applied to achieve large open spaces at lower floors for pluralistic commercial facilities such as parking lots, shopping centers, and metro stations. As transmitting loads from the top to the supporting columns or walls, transfer structures can be defined as either flexural or shear structure [1]. A transfer story has several types, for example, transfer beam (girder) [1], transfer slab (plate) [2–7], or transfer box [8], among which the transfer slab structure is quite popular due to being free from the limitation of the forms of the upper and lower structures and the flexible axes distribution of upper and lower stories. Due to the space requirement of subway station, the height of frame structure differs greatly from the first floor to the second floor, resulting in structural stiffness mutation and the formation of soft-story [9–27]. Buildings with soft-story had a significantly higher proportion of serious damage than other conventional types of

buildings after the earthquake in Hyogo-ken Nambu (1995) as well as in Mexico City (1985) [7]. The internal force of the vertical anti-lateral component of the structure is transferred downward by the horizontal conversion component, and the structure displays obvious vertical irregularity [9–27]. The plate–column joints of this structure have complex forces under seismic loads; therefore, some scholars have carried out studies on such structures from the perspective of the joints [4–6,28–36].

The structural performance of a low-rise building with a transfer beam in Hong Kong under probable seismic events was examined by Li JH [1]. Xiangming Zhou [2] analyzed the performance of high-rise buildings with transfer panels under wind and earthquake action; the results showed that seismic action should be clearly considered in design in areas with moderate seismic activity. Su R [3] provides a method for assessing the structural performance of transfer structures in the face of prospective seismic events. The results revealed that the mega-columns supporting the transfer plate and the coupling beams at higher zones are the most vulnerable components in the event of a seismic event. Su-min Kang [4] conducted an experimental study on the punching shear strength of conversion slabs with different forms of reinforcement and discovered the use of diagonally reinforced upper plate increased the punching shear strength of conversion slab specimens by 100–128% [4–6]. Three 1:12 scale 17-story RC wall building models were subjected to the same sequence of simulated earthquake excitations to examine their seismic response characteristics. Based on the test results, the anticipated fundamental periods in UBC 97 and AIK 2000 for structures other than moment frames and bearing wall constructions appear to be realistic [7].

Previous studies have made some achievements in theoretical analysis and dynamic characteristics of structures, which are of great significance to subsequent scientific research and engineering practice. However, the development of stress and strain, the damage and cracking characteristics of complete frame-supported shear wall structure with transfer slab under low cycle reciprocating load are not discussed. Based on the above problems, in order to investigate the seismic capacity and damage development features of complete frame-supported shear wall structure with transfer slab in high-rise buildings under earthquake action, a 1/5 large space structure model was designed for pseudo-static test. On the one hand, the research can verify whether this type of structure can meet the requirements of seismic performance under the action of various seismic levels; on the other hand, it can study the damage development and strain characteristics of the structure.

## 2. Test Overview

### 2.1. Specimen Design

The original structure of the experiment model (Figure 1) is a 30-story transfer slab structure with a height of 102.1 m, the first story is the subway parking garage, the second story is the car garage; the first and second stories are the frame structure, the third story and above are the shear wall structure, where the frame and shear wall are connected by transfer slab. As the original structure (Figure 1) has many cross units and is limited by the space conditions of the test site, a simplified structure (Figure 2) was designed to reflect the seismic performance, deformation characteristics, and failure characteristics of the original structure. During the simplification process, the section size of the component did not change. The number of spans was reduced and shear walls were arranged in a manner that is most unfavorable to mid-span columns and plates.

The simplified structure is scaled down according to the similarity ratio of 1:5. The experiment model with large scale ratio can more intuitively reflect the damage and cracking of the original structure. However, due to the limitation of the space conditions of the test site, the whole building model after scale reduction cannot be taken for experimental research. To study the seismic performance of the transfer thick plate structure, the 1st to 5th floors after scale reduction were taken as the research object (Figure 3). A concrete equivalent mass block was set at the top of the fifth floor, which was used to simulate the vertical gravity action of the upper shear wall structure (Figure 3) because its gravity

meets the counterweight requirements of the shear wall on the fifth floor. The seismic performance of the transfer slab is different in the tower area and non-tower area, so it needs to be treated differently in design. In the tower area, the transfer slab is 260 mm thick, and the frame columns under the thick plate are adopted steel concrete columns; the transfer slab in the non-tower area is 70 mm thick, and the frame columns under the sheet are reinforced concrete columns; hidden beams (beams arranged inside a thick plate) are arranged at the junction of thin plate and thick plate to solve the problem of stress concentration.

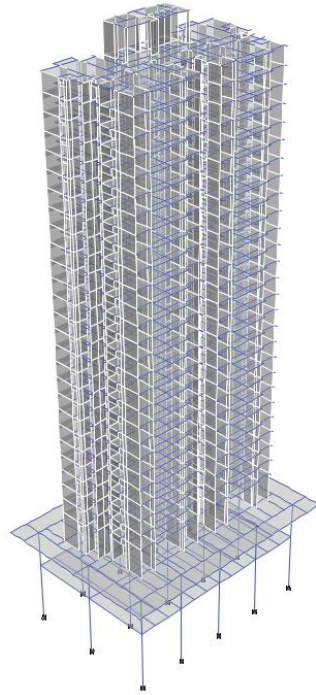


**Figure 1.** Original structure modeling.

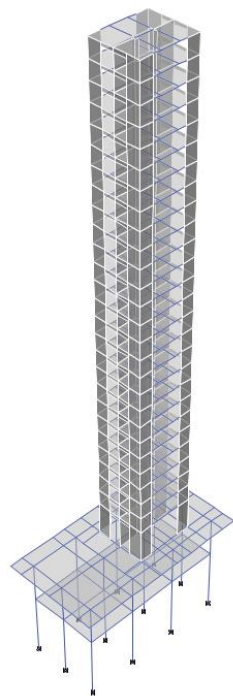


**Figure 2.** Simplified structure modeling.

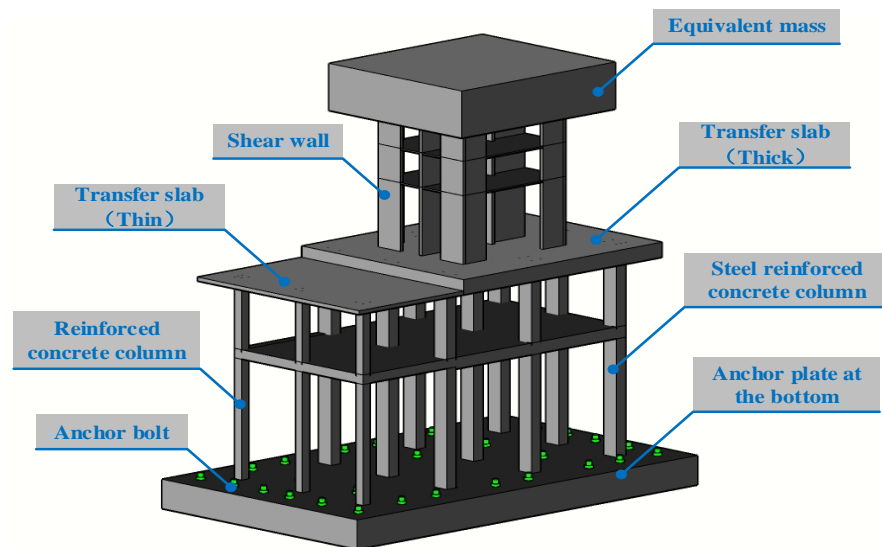


Figure 3. Experimental object.

Table 1 shows the scale model and the height of each floor of the original structure. The design strength of the experiment model concrete is C30. The reinforcement ratio of frame structure and transfer slab is the same as that of the original structure, using Q345 I-steel, HRB400 steel bar (diameter 6, 8, 10, 12, 14 mm), and 8# steel wire. The shear wall structure section of the model is too small to arrange steel bars as the research needs. Therefore, when designing the upper shear wall structure model, the internal steel bars should be replaced by 8# steel wire (diameter 4.06 mm) on the premise of the same strength ( $A_b \cdot \sigma_b = A_w \cdot \sigma_w$ ,  $b = \text{steel bars}$ ,  $w = \text{8\# steel wire}$ ). The mass block at the top of the 5th floor is made entirely of concrete, the reinforcement diagram and layout of the test model are shown in Figures 4–6. A similar relationship is shown in Table 2.

Table 1. Story height and additional weight.

Type	Simplified Structure			Experimental Object			
	Story	Story Height (m)	Floor Mass (t)	Story	Story Height (m)	Floor Mass (t)	Counterweight (t)
Shear wall	5~29	2.9	$120.4 \times 25$	5	0.58	0.71	23.29
Shear wall	4	2.9	132.1	4	0.58	0.81	0.25
Shear wall	3	5.8	181	3	1.16	1.24	0.21
Frame column, Transfer slab	2	7	2512.2	2	1.4	13.14	6.96
Frame structure	1	11	834.1	1	2.2	6.5	0.17

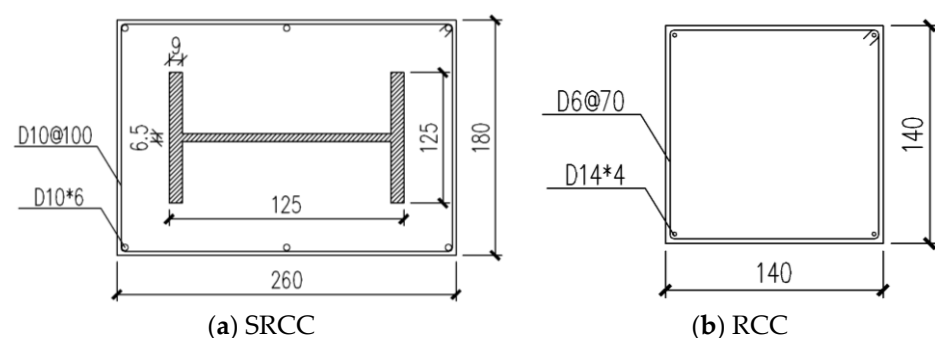
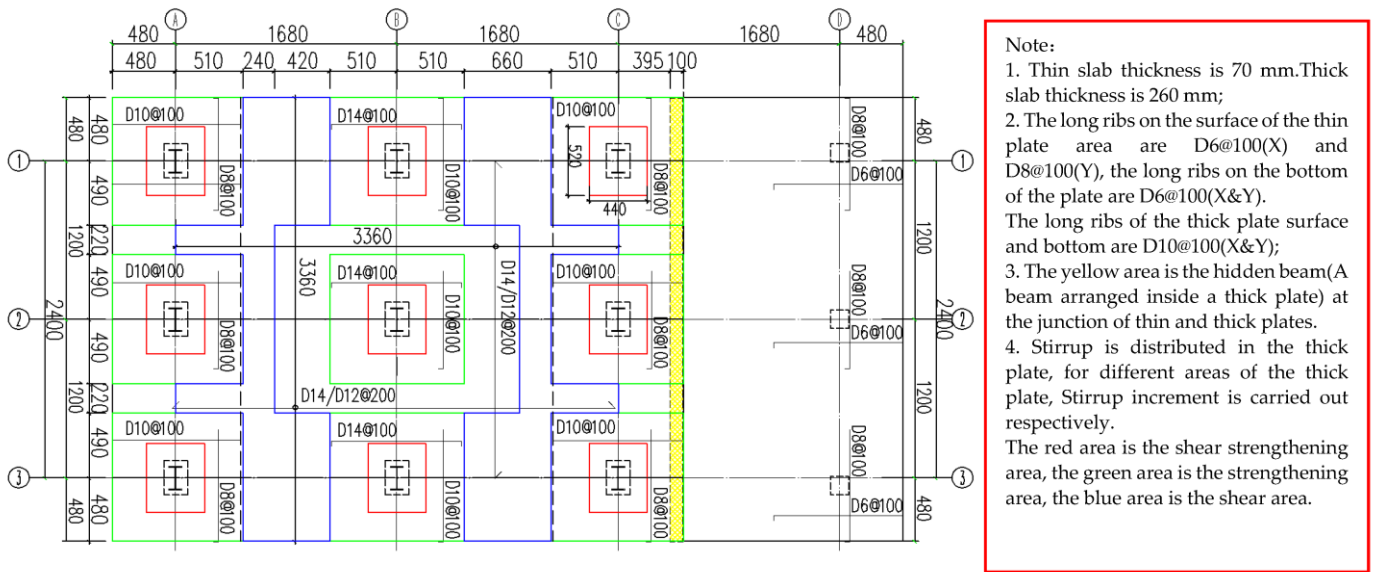
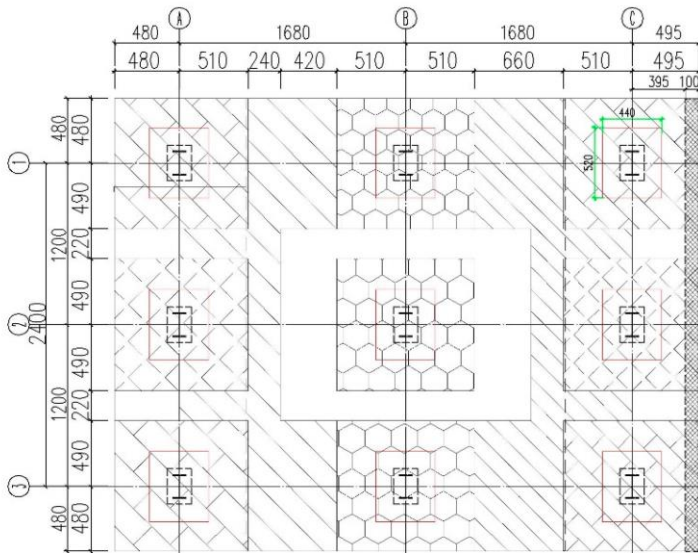


Figure 4. Column reinforcement diagram.



(a) Longitudinal reinforcement



(b) Stirrup (hooping)

Figure 5. Transfer plate reinforcement.

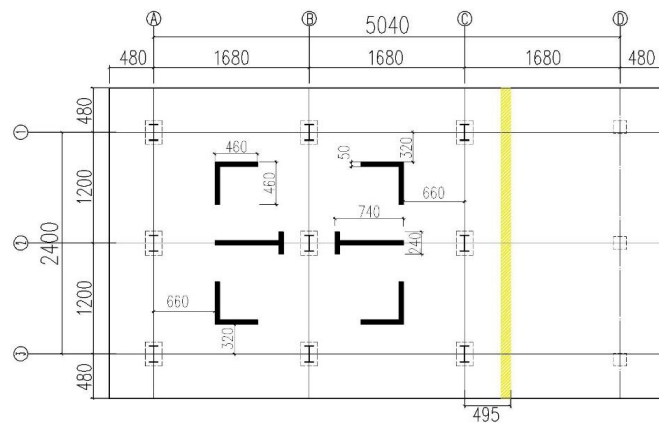


Figure 6. Shear wall layout plan.

**Table 2.** Similar relationship.

Physical Quantity	Formula	Similar Relationship
Size (m)	$S_L = h_s/h_o$	1:5
Density (kg/m <sup>3</sup> )	$S_\rho = \rho_s/\rho_o$	1:1
Mass (kg)	$S_m = \rho_s V_s / \rho_o V_o = S_\rho \cdot S_L^3$	1:125
Reinforcement ratio (%)	$S_{\rho_1} = \rho_{1s}/\rho_{1o}$	1:1
Strain	$S_\epsilon = \epsilon_s/\epsilon_o$	1:1
Displacement (mm)	$S_x = \epsilon_s l_s / \epsilon_o l_o = S_\epsilon \cdot S_L$	1:5
Force (kN)	$S_F = F_s / F_o = A_m \cdot \sigma_m / A_o \cdot \sigma_o = S_L^2 S_\sigma$	1:25
Bending moment (kN·m)	$S_M = F_m L_m / F_s L_s = S_F \cdot S_L$	1:125

Note: Footnote “s” is the scaled model, footnote “o” is the original model.

## 2.2. Loading Programs and Institutions

### 2.2.1. Vertical Loading

During the experiment, the axial compression ratio of the structure should be satisfied, vertical loading is done by adding weights. (The vertical loading is the dead load). According to the stress similarity condition, the mass similarity ratio of the model is 1:125, and the gravity similarity ratio is 1:25. The counterweights of each story of the experiment model are listed in Table 1, and are arranged on stories 1–4, respectively. The concrete mass block at the top of the fifth story is poured in an integrated way, as shown in Figure 3. The concrete mass block meets the counterweight requirements of the fifth story.

### 2.2.2. Horizontal Loading

Two actuators (Model: ZB-300 t, Range: +3000 kN, −1300 kN) were used for horizontal loading, which were respectively arranged on the first story and the second story of the test model. According to the Chinese Seismic design Code [37] (p. 33), the seismic fortification intensity in Guangzhou is 8 degrees. With reference to the maximum horizontal earthquake influence coefficient in the specification (Table 3), the response spectrum method of mode decomposition was adopted to calculate the inter-story shear force and floor displacement of the model under different earthquake actions, so as to obtain the loading displacement. Horizontal loading is carried out after overturning moment loading, including two stages of preloading and formal loading. In the pre-loading stage, force control is adopted for each stage of loading cycle once to ensure that all equipment is in normal working state. Experimental loading is carried out and controlled by displacement, and the loading mode is three times for each stage. The loading regime is shown in Table 4 and Figure 7.

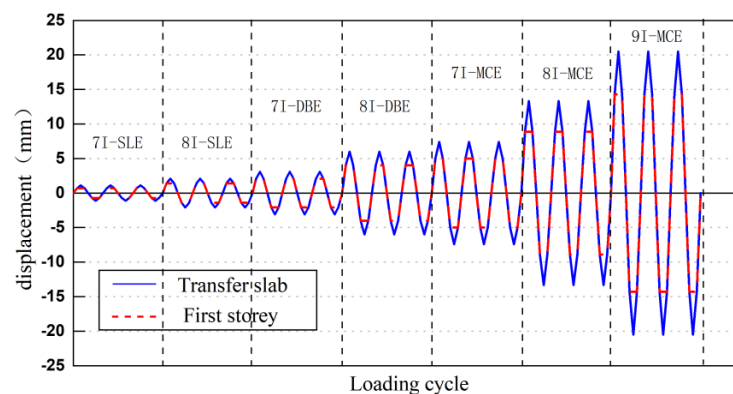
**Table 3.** Maximum horizontal seismic influence coefficient.

Seismic Response	7 Intensity <sup>1</sup>	8 Intensity <sup>1</sup>	9 Intensity <sup>1</sup>
Service level earthquake	0.08	0.16	0.32
Design based earthquake	0.23	0.45	0.9
Maximum considered earthquake	0.50	0.90	1.4

<sup>1</sup> The acceleration of the earthquake in the 7 intensity area is 0.1 g. The acceleration of the earthquake in the 8 intensity area is 0.2 g. The acceleration of the earthquake in the 9 intensity area is 0.4 g.

**Table 4.** Load regime.

Loading Regime	Jack Loading Displacement	First Story Actuator Displacement/Force (Inter Floor Displacement Angle)	Transfer Story Actuator Displacement/Force (Inter Floor Displacement Angle)
1 (Preload-1)	±0.1 mm	1 kN	5 kN
2 (Preload-2)	±0.15 mm	2 kN	10 kN
3 (Preload-3)	±0.2 mm	4 kN	20 kN
4 (7I-SLE)	±0.265 mm	±0.7 mm (1/3143)	±1.1 mm (1/3500)
5 (8I-SLE)	±0.455 mm	±1.4 mm (1/1571)	±2.1 mm (1/2000)
6 (7I-DBE)	±0.49 mm	±2.1 mm (1/1048)	±3.1 mm (1/1400)
7 (8I-DBE)	±1.16 mm	±4 mm (1/550)	±6 mm (1/700)
8 (7I-MCE)	±1.29 mm	±5 mm (1/440)	±7.4 mm (1/583)
9 (8I-MCE)	±2.345 mm	±8.9 mm (1/247)	±13.3 mm (1/318)
10 (9I-MCE)	±4.589 mm	±14.3 mm (1/154)	±20.5 mm (1/226)

**Figure 7.** Horizontal loading mode.

### 2.2.3. Overturning Moment of Superstructure

Multiple earthquake damage investigations show that the overall collapse of the building structure is quite serious due to the second-order gravity effect of superstructure [7], so the influence of the overturning moment of the superstructure under the earthquake must be considered in the test. In order to meet the loading requirements of overturning moment, a cast-in-place reinforced concrete counterforce frame was designed (Figures 8 and 9). The bottom of the counterforce frame was fixedly connected to the ground by anchorage bolts. Four jacks (Model: LZDF-500 t, Range: +5000 kN) were fixed on the four beams of the counterforce frame by connecting pieces (as shown in Figures 9 and 10). Steel plate was embedded where the equivalent mass contacts the jack (as shown in Figure 9), the surface of the steel plate was coated with lubricant, and the horizontal movement of the equivalent mass was not restricted by the reaction frame. When the actuators on the first and second floors were under positive loading, anti-symmetric displacement loads were simultaneously applied to the Jack-1 and Jack-4. When the actuator was negatively loaded, Jack-2 and Jack-3 were simultaneously subjected to antisymmetric displacement loads, and

the loading displacement of the jack was obtained by the angle of fifth floor calculated by the mode-superposition response spectrum method, as shown in Table 4. Overturning torque loading includes two stages: pre-loading and formal loading. In the pre-loading stage, force control was adopted for each stage of loading cycle once. After ensuring that all equipment was in normal working state, formal loading was carried out. The formal loading was controlled by displacement, and the loading cycle was three times for each stage. The loading regime is shown in Table 4 and Figure 8.

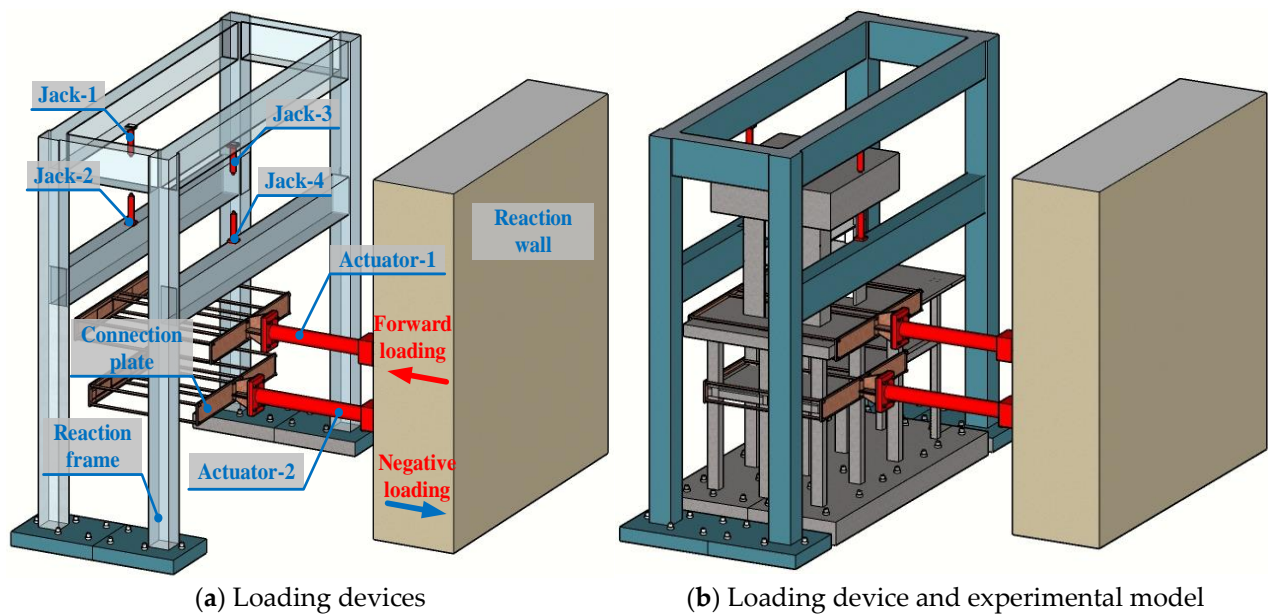


Figure 8. Schematic diagram of loading device and experimental model.

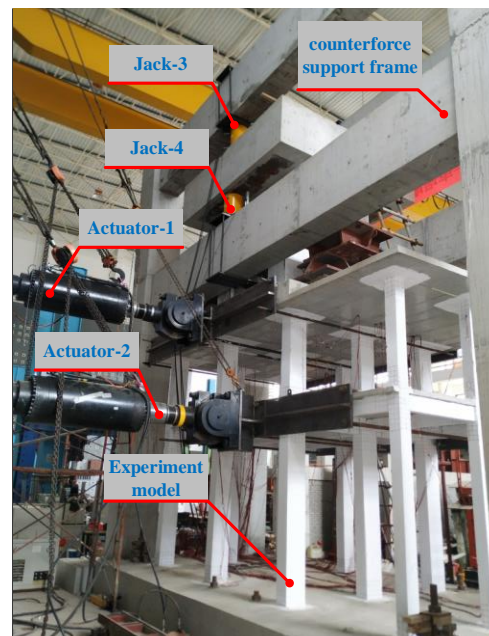


Figure 9. Experimental model.

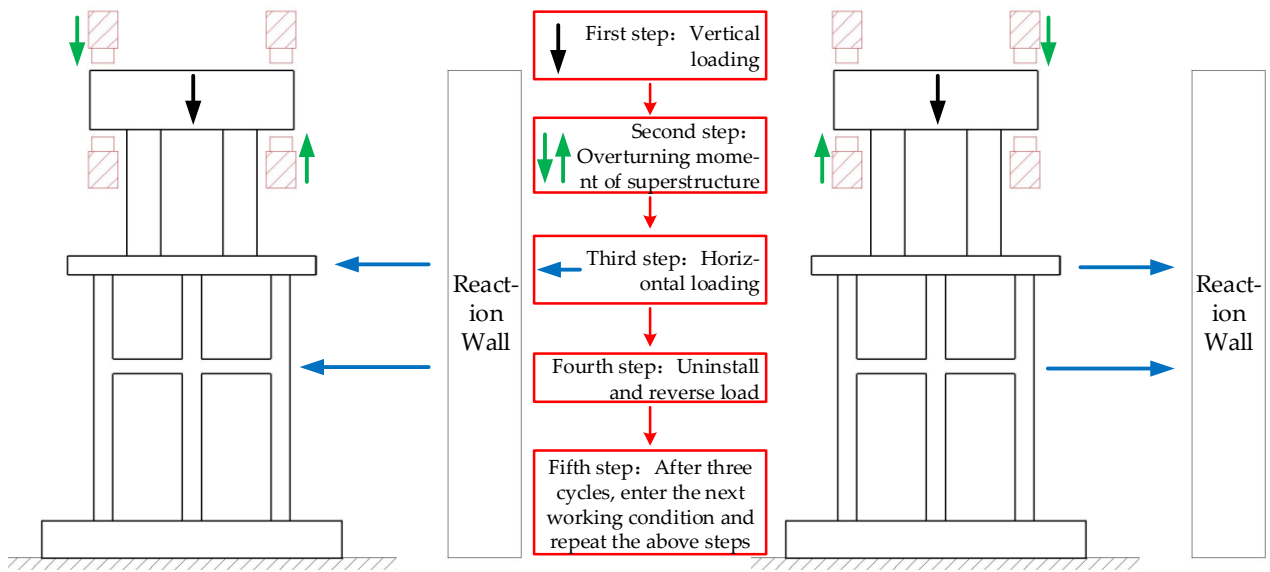


Figure 10. Loading diagram (the left image is positive loading and the right image is negative loading).

2.3. Collection Strain

To monitor the deformation of the bottom frame column, strain gauges were arranged at the section steel, longitudinal reinforcement, and stirrup at each column node of axis 2, as shown in Figure 11. Moreover, strain gauges were also arranged on the longitudinal reinforcement and stirrup in different areas of the conversion plate to monitor the deformation of the transfer slab, as shown in Figure 12. In the figure, red parts refer to the strain gauge arranged on the section steel, blue parts refer to the strain gauge arranged on the stirrup, and green parts mean the strain gauge arranged on the longitudinal reinforcement. The diameter of steel wire in the upper shear wall structure was too small to arrange strain gauge.

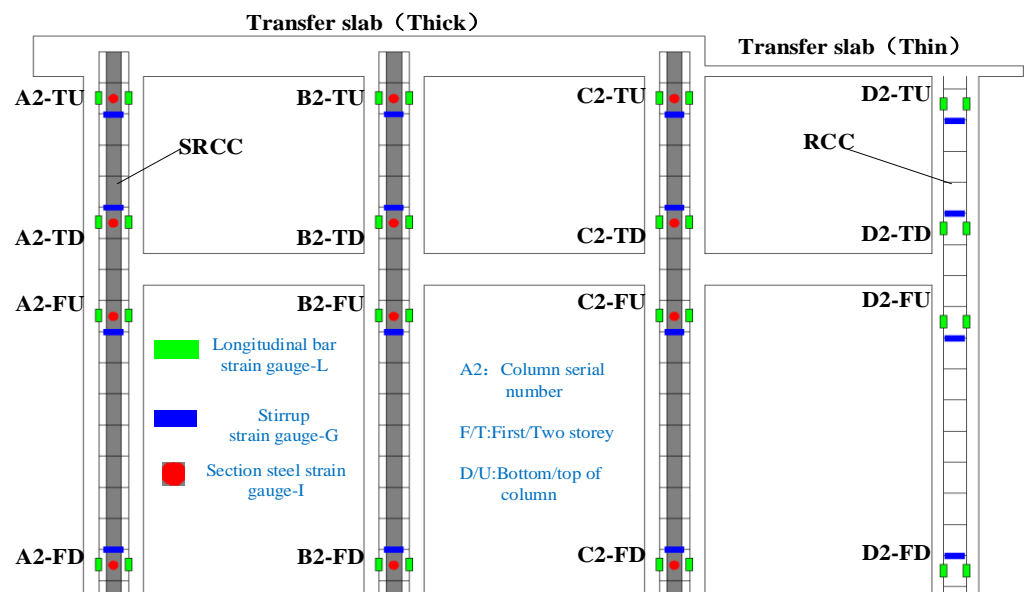


Figure 11. Frame column strain layout plan.

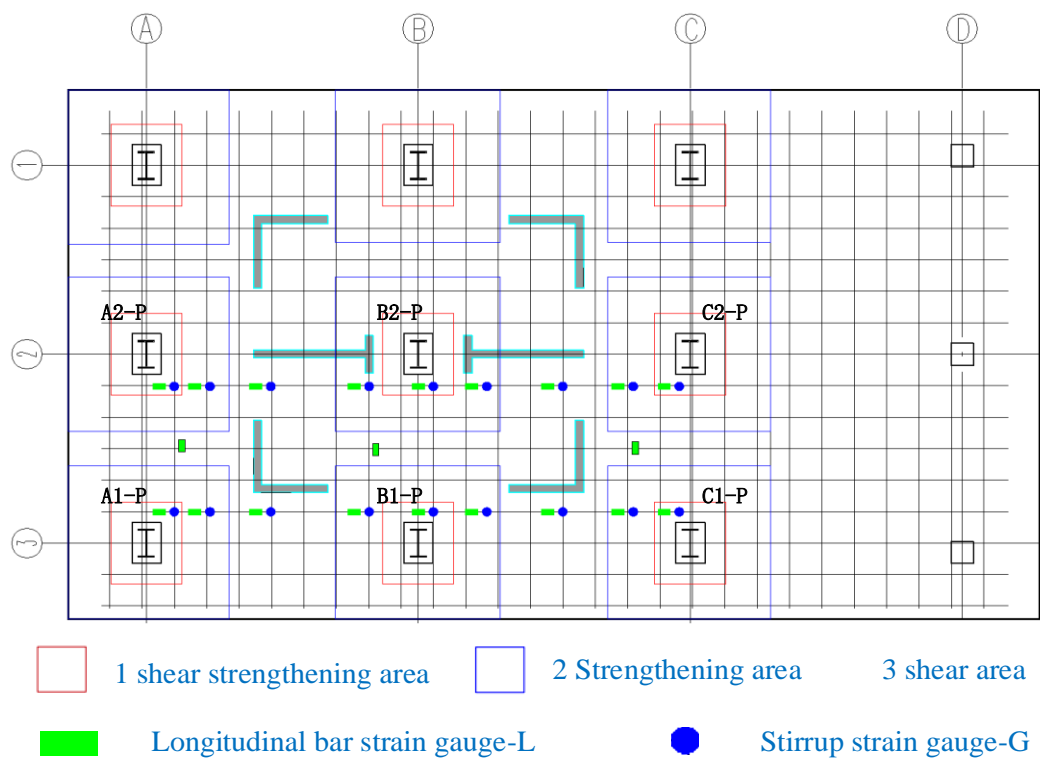


Figure 12. Transfer slab strain layout.

### 3. Experiment Results

7I-DBE damage condition: No cracks were observed in the 7I-SLE and 8I-SLE conditions. Under the 7I-DBE conditions, cracks were first observed in the middle area of the three-story shear wall body, and then subtle cracks appeared in the upper area of the first story column, but no cracks were observed in the second story and the transfer slab, as shown in Figure 13.

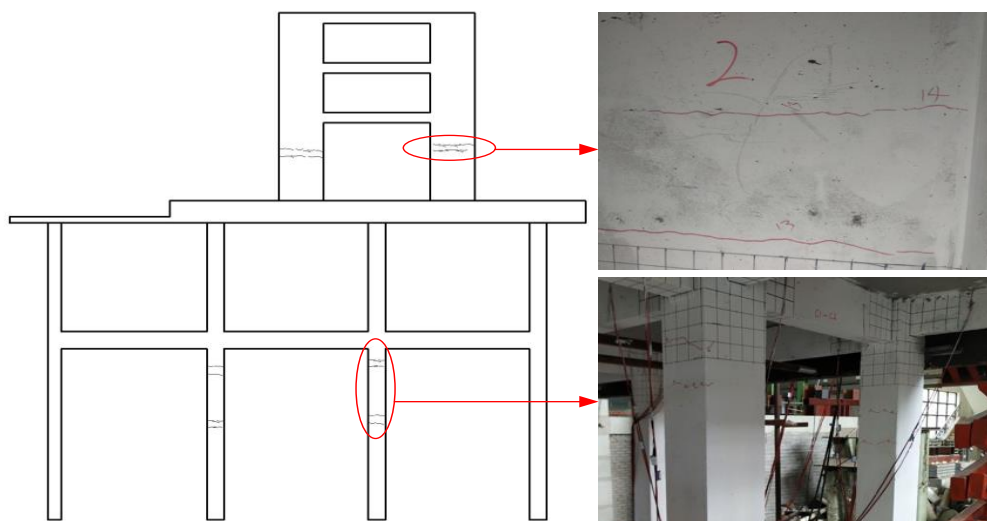
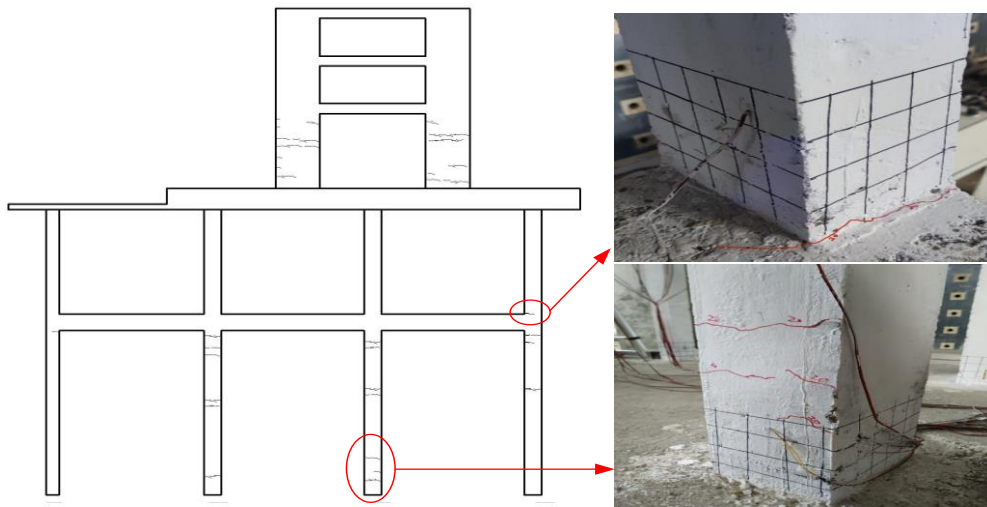


Figure 13. 7I-DBE damage condition.

8I-DBE damage condition: the cracks of the columns on the first floor increased, and the cracks appeared at the bottom of the columns for the first time. Meanwhile, cracks appeared on the lower surface of the beam on the first floor, subtle cracks appeared on the node position at the bottom of the columns on the second floor both for the first time, and

the cracks extended to the surface of the slab on the first floor. Cracks increased on the shear wall of the third floor, as shown in Figure 14.



**Figure 14.** 8I-DBE damage condition.

7I-MCE damage condition: The column cracks of the first floor continued to increase, the beam and column nodes of the first floor showed new cracks, the slab surface cracks of the first floor also continued to develop. Horizontal cracks were found at the top of the frame columns on the second floor, but no cracks were observed in the transfer slabs. Cracks increased in the shear walls on the third floor, as shown in Figure 15.

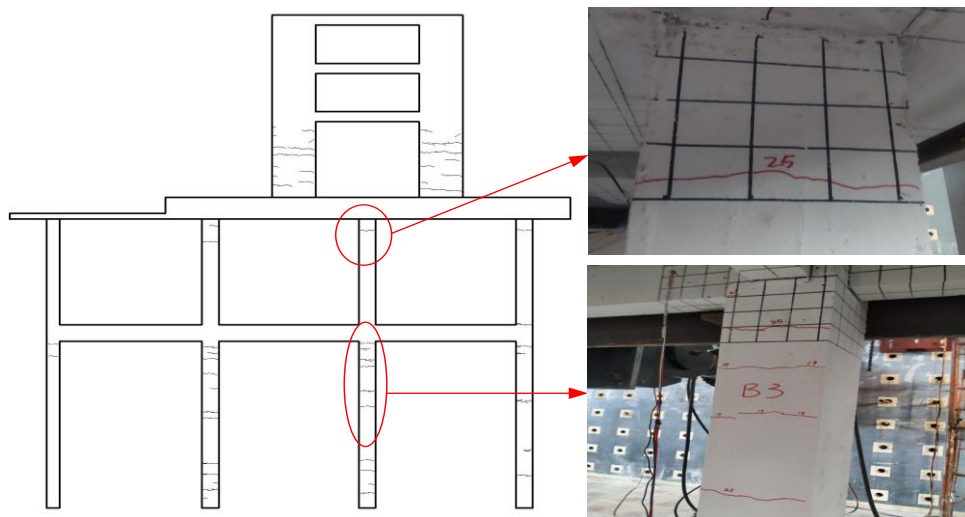


**Figure 15.** 7I-MCE damage condition.

8I-MCE damage condition: The columns on the first floor were seriously damaged, with many long cracks appearing, and new cracks appearing at the embedded ends of the columns at the bottom. There were more horizontal cracks on the top of the second-floor columns, but no cracks were found in the transfer slabs. There were more new cracks in the shear wall and the original cracks continued to develop, as shown in Figure 16.

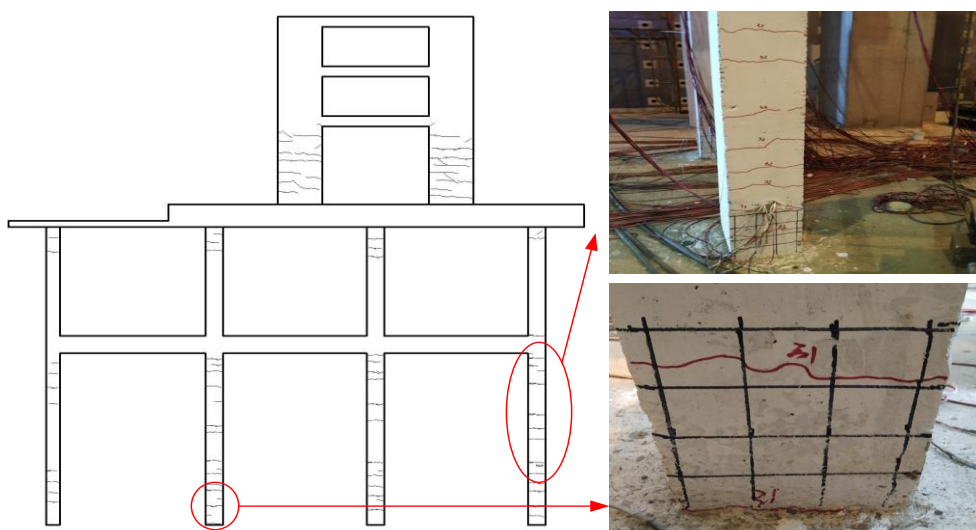
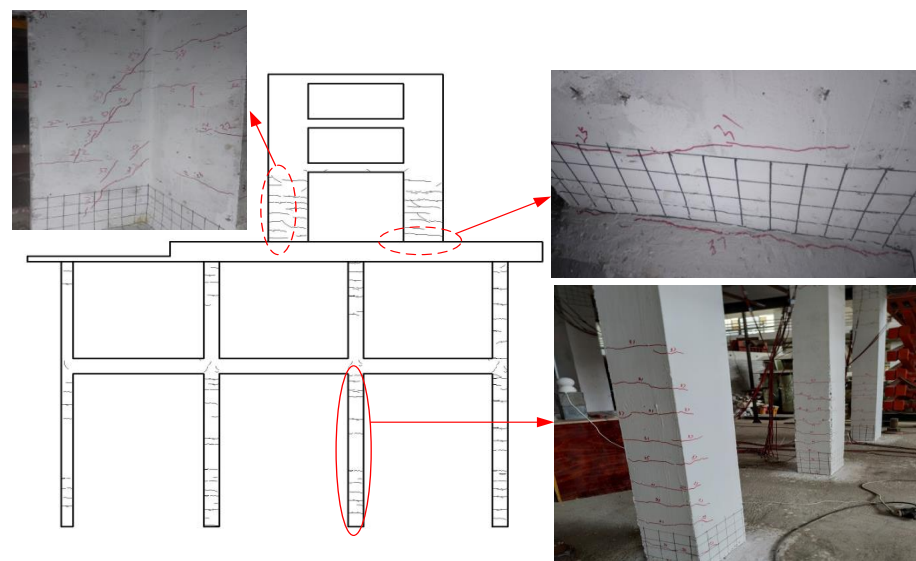


**Figure 16.** 8I-MCE damage condition.

9I-MCE damage condition: Under the 9I-MCE condition, the damage of the first floor was more serious, and cracks appeared at the embedded ends of each column. A horizontal crack with a width of 0.3 mm appeared at the junction between the top of B2 column and the slab for the first time, and a full-length crack appeared at the top and the bottom of slab on the first floor. A large number of new cracks appeared on the top of the columns on the second floor, but no cracks were found on the transfer slab, numerous inclined cracks appeared on the shear wall on the side, and the embedded end of the shear wall was seriously cracked, as shown in Figure 17b,c, which shows the detailed damage diagram of some nodes of the structure under the 9I-MCE condition. The failure of the beam or beam joint can consume energy during the earthquake and reduce the adverse effect of the earthquake on the column. Therefore, in the initial design, the engineers wanted to destroy the beam joints in the frame structure. However, it was found from the experiment results that although cracks were generated in the beam-column joints under the 9I-MCE condition, the damage to the beams or beam joints was not serious, which does not reach the expected design idea. The reason may be that the binding of the connecting plate on the first floor was too strong, resulting in the rotation of the floor being limited.

The story drift ratio (ratio of story displacement to story height) of the transfer slab was 1/226, and that of the first story plate reached 1/154. The safety performance of the structure met the seismic requirements of a nine-degree earthquake. The first-floor frame column and shear wall suffered the most serious damage, while in the meantime, the beam and plate had less damage. The columns of the second floor developed many cracks under the nine-degree earthquake, but no cracks ever appeared in the transfer slab.

The first-floor frame columns cracked earlier and more seriously than the second floor; therefore, the first-floor frame may be the weak part of the bottom frame structure. The three-story shear wall structure of the tower part also cracked earlier and more seriously than the frame floor. Under the action of load, a reasonable damage mechanism is formed that the members above the transfer story cracked first and those below the transfer story cracked later. According to the damage of the structure, it can be judged [38] (pp. 128–135) that the damage condition of the bottom frame structure was between (a) intact and (b) slightly damaged. The shear wall of third floors of tower structure with damage between (b) minor damage and (c) light and moderate damage, which shows that the performance goal of the structure below the transfer story was higher than that above the transfer story. The design concept “the performance goals at the bottom of the frame structure is higher than that at the upper shear wall structure” was satisfied.



(a) 9I-MCE damage condition



(b) The damage was aggravated at the beam-column joints



(c) The bottom of the first floor appeared horizontal through long cracks

**Figure 17.** 9I-MCE damage condition.

#### 4. Component Strain Analysis

##### 4.1. Strain Analysis of Frame Structure

In order to avoid the disadvantage of the bottom frame failing before the upper shear wall, leading to the overall overturning of the structure, when designing the seismic performance objectives of structure, the performance target of the structure below the transfer story was higher than that of the structure above the transfer story [38]. In the original structure of the model, the performance objective of the structure below the transfer story was determined as B, and that of the structure above the transfer story was determined as C (the seismic performance objectives were divided into four grades from high to low: A, B, C, and D).

Figure 18 shows the strain curve of the frame column. In the figure, the horizontal coordinate is the loading displacement value of the No. 1 actuator, and the vertical coordi-

nate is the strain. It can be seen from the figure that during the whole loading process, the strain of steel bar was less than its yield strain (HRB400 steel bar yield strain was  $2000 \mu\epsilon$ , the boundary of the Y-axis of the strain diagram was the yield strain), and according to the above failure phenomenon, there was no oblique crack on the column surface, indicating that the seismic performance levels of structure below the transfer story met the requirements of performance level 3 under maximum considered earthquake (MCE) [38] (p. 7). From this conclusion, it can be judged that the bottom frame structure reached the requirements of performance objective B, indicating that the seismic performance of the bottom frame structure was higher than the performance objective C of the structure above the transfer story. It met the design concept of “the performance goal of the bottom frame structure is higher than that of the upper shear wall structure”, so the bottom frame was still in the elastic stage and met the expected design goal.

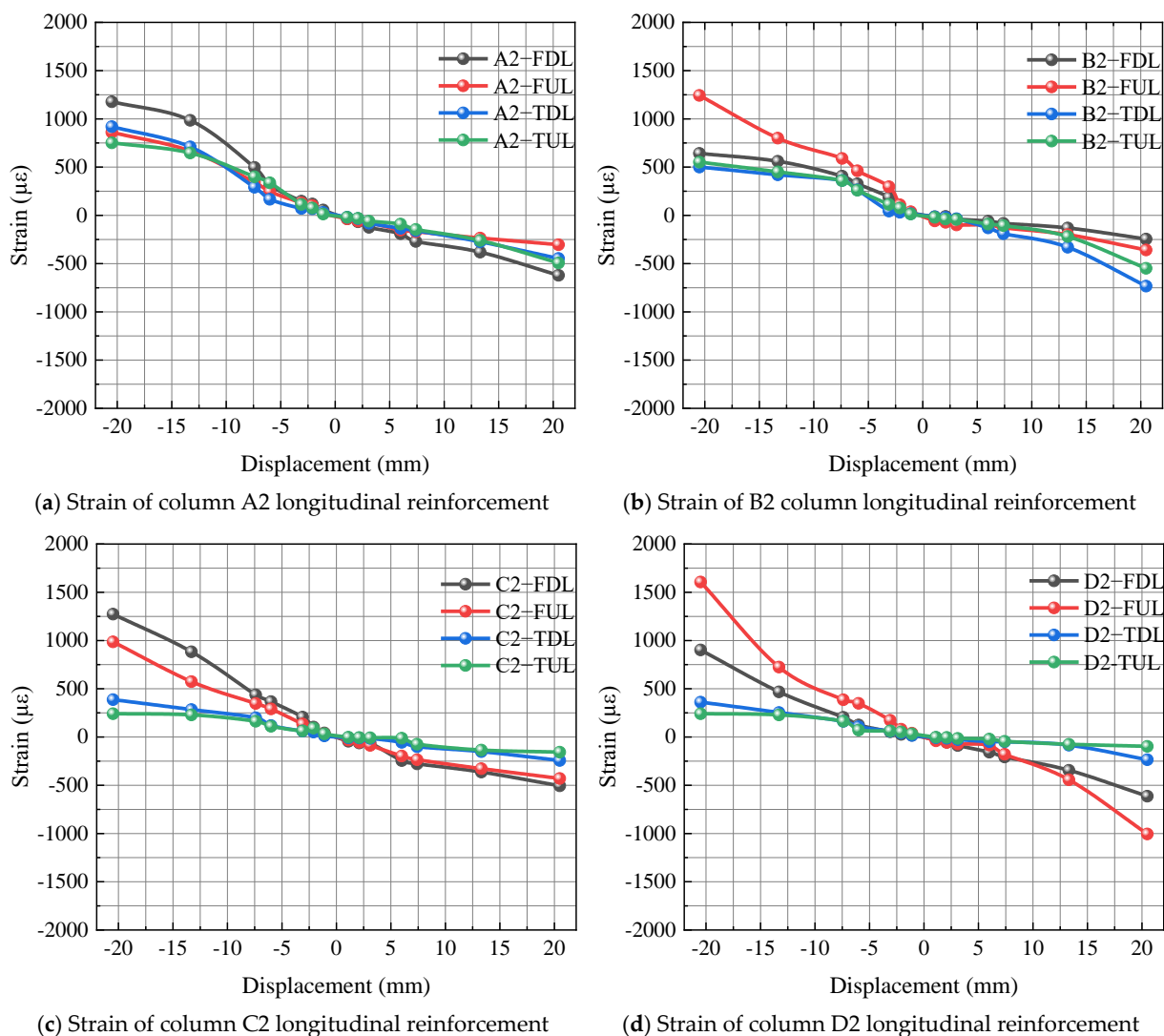


**Figure 18.** Longitudinal reinforcement strain of frame column.

The strain of the longitudinal reinforcement of the first story was higher than that of the second floor, and the first story was still the weak part of the bottom frame. In many areas, the failure of the soft-story of the structure caused the overall collapse of the building. In order to avoid this phenomenon, the seismic performance target of the bottom frame structure was raised one level in the design of the structure. This design concept can make the structure show a reasonable damage mechanism of “members above the transfer story yield first, and members below the transfer story yield later”.

#### 4.2. Strain Analysis of Transfer Slab

Figures 19 and 20 show the strain of reinforcement in the transfer story, and the reinforcement was in an elastic state during the whole loading process. The stirrup strain increased significantly under the nine-degree earthquake condition, and the stirrup strain in the thick plate near the shear wall was much higher. In the process of positive loading, the overturning moment of the superstructure led to a significant increase in the stirrup force at the junction of shear wall and transfer plate. The strain of the longitudinal reinforcement fluctuated around 0, and the maximum strain of stirrup was  $1775 \mu\epsilon$ , the stirrup strain was higher than the longitudinal strain, and the transfer story was mainly deformed by shear force. The stirrup strain in the transfer story was large and there was no crack on the surface, which indicates that the transfer story may form shear failure (brittle failure). This adverse failure mechanism needed to be avoided by providing sufficient strength on the one hand, and by reasonable design on the other hand, so that the yielding floor appeared at the bottom strengthening site above the transfer story. Therefore, the design should focus on the design concept of “the performance goal of the bottom frame structure is higher than that of the upper shear wall structure”.

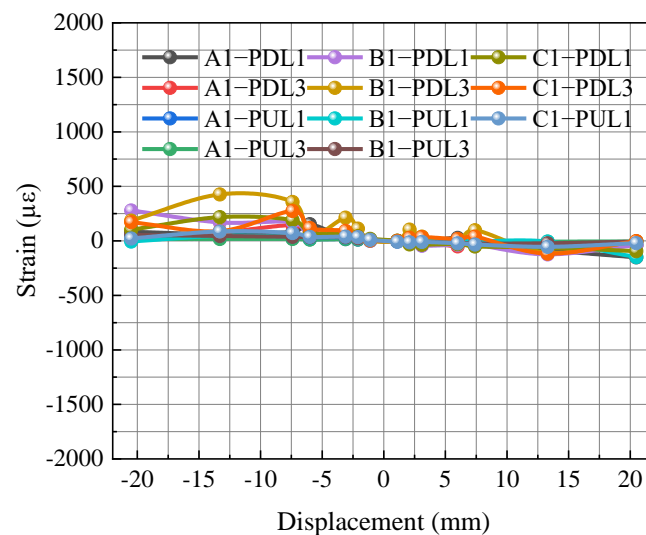


Figure 19. Strain of longitudinal bars in thick plates.

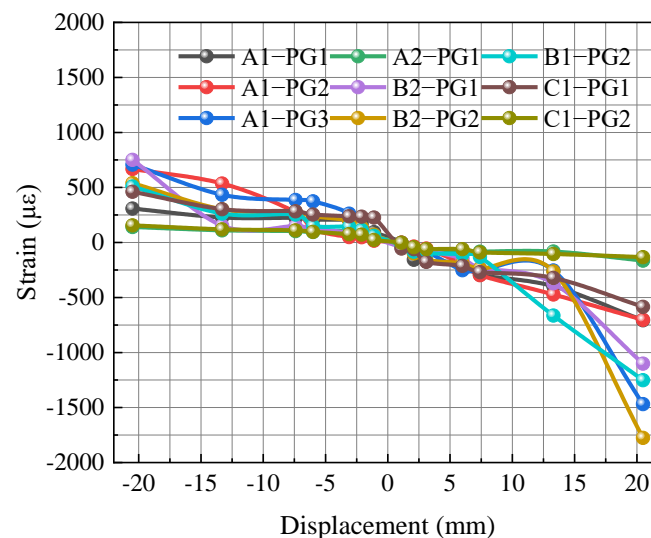
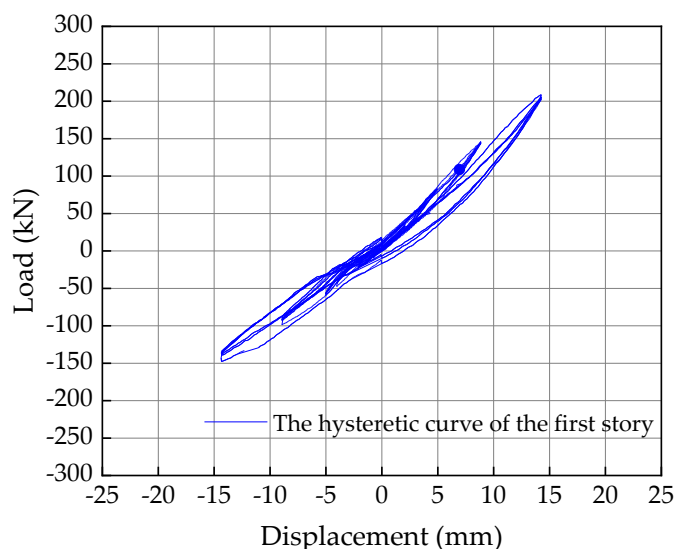


Figure 20. Strain of stirrups in thick plates.

## 5. Experiment Analysis

### 5.1. Hysteretic Performance

The hysteretic curve of the first story actuator is shown in Figure 21. Before loading in 9I-MCE condition, the loading path of the hysteretic curve almost coincided with the unloading path, and the residual deformation of the model was small. The area of the hysteretic curve was very small under 9I-MCE condition.



**Figure 21.** The hysteretic curve of the first story.

Figure 22 shows the hysteretic curve of the transfer story actuator. Due to the influence of the cooperative loading mode (meaning that both actuators were loaded simultaneously), the hysteretic curve of the transfer story showed a special “inverse S-shape”. At the beginning of loading, the first story’s actuator was loaded synchronously with that of the transfer story, the horizontal displacement of the transfer story was the same as that of the first story, and load was mainly provided by the actuators of the first story. At this stage, the hysteretic curve of the first story had a higher slope, while the hysteretic curve of the transfer story grew more slowly. When the synchronous loading was completed, the displacement of the first story actuator remained unchanged, and the actuator of the transfer story continued to increase the displacement load. At this time, the lateral resistance provided by the first story’s actuator decreased, and all the resistance originally provided by the first story’s actuator was provided by the actuator of the transfer story, so the hysteretic curve of the transfer story had a sudden change in slope at this stage. With the increase of load displacement, the area of hysteretic curve of the transfer story increased gradually. It can be seen that the area of hysteretic curve of the transfer story was obviously higher than that of the first story, and the loading path did not coincide with the unloading path. The loading path and unloading path of the hysteretic curve of the transfer story no longer coincided since the 7I-DBE started, which indicates that the model had already shown unrecoverable damage, which can also be verified by the cracking phenomenon of the model in the previous discussion.

Since the shape of hysteretic curve was affected by the cooperative loading mode, the cumulative energy consumption of the first story and the transfer story was not compared and analyzed. Instead, the cumulative energy consumption of both was superimposed, which can reflect the overall energy consumption of the bottom frame structure. Figure 23 shows the energy dissipation curve. Under the conditions of SLE and DBE, the damage of the structure was small, mainly elastic deformation, and less energy consumption. The energy dissipation curve of the model increased significantly under large earthquake conditions, and the total cumulative energy dissipation of the frame structure increased from 318.46 kN·mm at 7I-MCE to 3496.10 kN·mm at 9I-MCE.

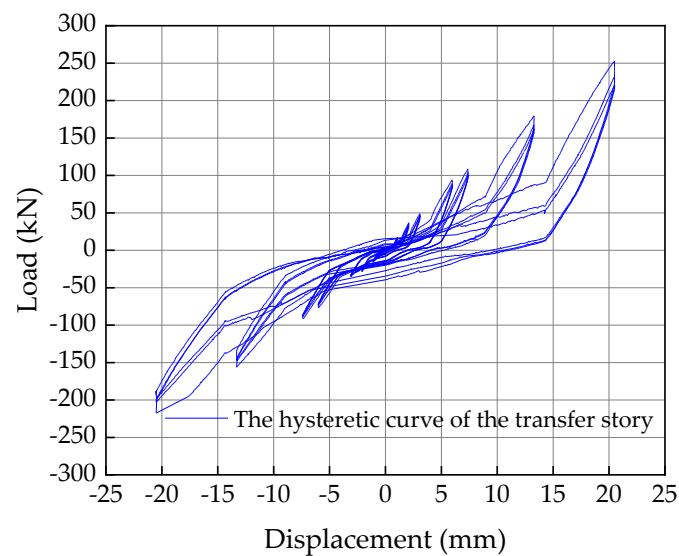


Figure 22. The hysteretic curve of the transfer story.

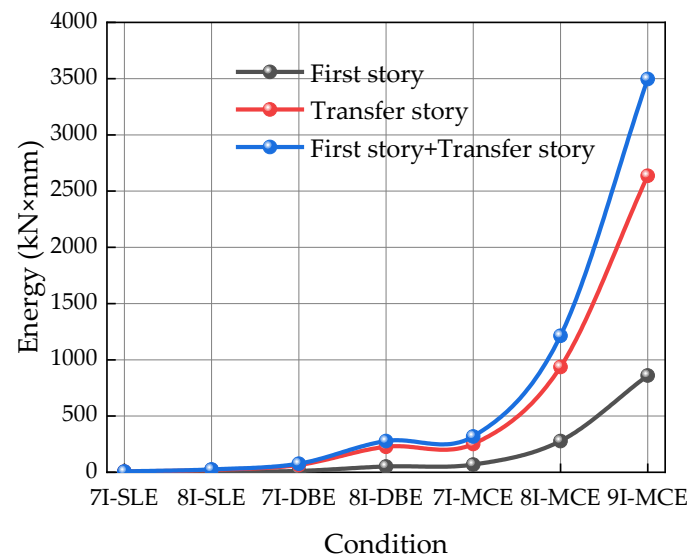
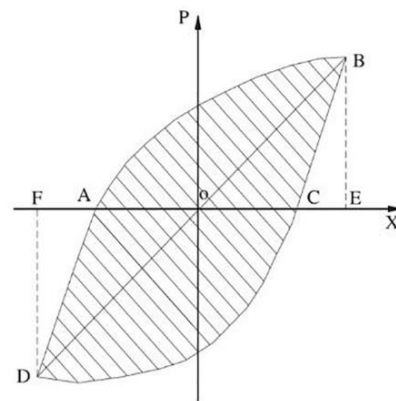


Figure 23. Energy-loading condition curve.

The equivalent viscous damping coefficient  $h_e$  is calculated using Equations (1) and (2), where  $S_{(ABC+CDA)}$  and  $S_{(OBE+ODF)}$  are the areas of the hysteretic curve. As shown in Figure 24 and Table 5, with the increase of load, the equivalent viscous damping coefficient (EVDC) of the transfer story rose, and the EVDC of the transfer story was larger than that of the first story.

$$E = S_{(ABC+CDA)} / S_{(OBE+ODF)} \quad (1)$$

$$h_e = E / 2\pi \quad (2)$$



**Figure 24.** Area chart of energy consumption capacity.

**Table 5.** Equivalent viscous damping coefficient.

Loading Conditions	Equivalent Viscous Damping Coefficient of the First Story	Equivalent Viscous Damping Coefficient of the Transfer Story
7I-SLE	2.67%	5.63%
8I-SLE	2.85%	4.85%
7I-DBE	3.22%	8.05%
8I-DBE	3.71%	7.52%
7I-MCE	3.01%	5.60%
8I-MCE	4.07%	6.67%
9I-MCE	5.45%	9.26%

With loading from 7I-MCE condition to 9I-MCE condition, the EVDC of the first story and the transfer story showed a slow increase. This indicates there was a large amount of irrecoverable damage in the structure, which also led to the increase of the EVDC of the structure. The maximum value of EVDC was 9.26% under the MCE conditions.

### 5.2. Skeleton Curve and Secant Stiffness

Figure 25 shows the skeleton curve of the model. (The skeleton curve is the track of the maximum horizontal force peak reached by each cyclic loading, which reflects the different stages and characteristics of the stress and deformation of the component). Figure 26 shows the secant stiffness of the model. (Due to the gap between the connector and the actuator, the secant stiffness fluctuated at the initial stage of loading. When the gap was eliminated, the secant stiffness showed a downward trend with the increase of loading displacement. This paper only analyzes the secant stiffness under the action of large earthquakes). The secant stiffness is calculated by Equation (3).

$$K_i = \frac{|+F_i| + |-F_i|}{|+X_i| + |-X_i|} \quad (3)$$

where  $F_i$  is the maximum peak load of hysteresis curve in the first turn of each working condition, and  $X_i$  is the maximum peak displacement of hysteresis curve in the first turn of each working condition.

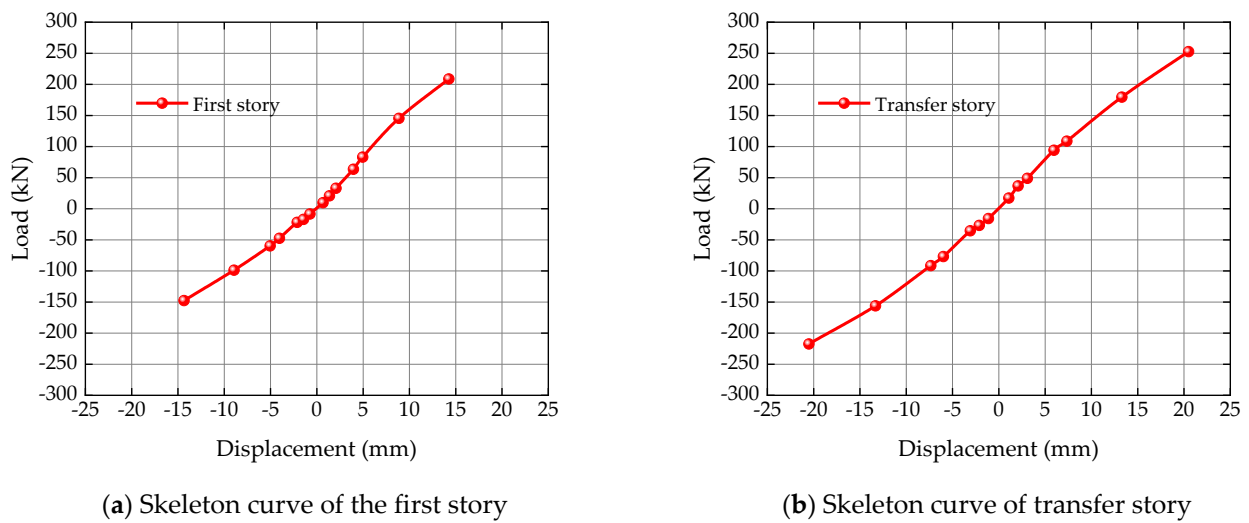


Figure 25. Skeleton curve.

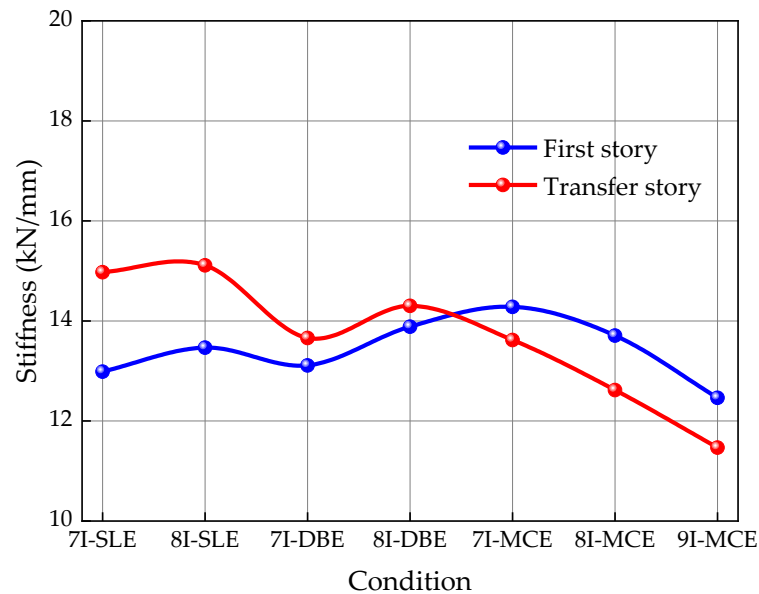


Figure 26. Secant stiffness curve.

The skeleton curve did not decrease during the loading process. Under the MCE condition, the slope of skeleton curve decreased, and the secant stiffness showed a downward trend with the increase of displacement. (The secant stiffness is equivalent to the slope of the skeleton curve. Therefore, when the slope of the skeleton curve decreased, the secant stiffness showed a downward trend, but the skeleton curve did not decrease). This indicates that the concrete of the frame structure columns had a lot of damage, which is consistent with the experimental results (Figures 13–17) mentioned above.

The bottom frame of the structure was mainly elastic deformation under the SLE and DBE conditions. Under the MCE condition, the reinforcement of the bottom frame of the structure was still in the elastic stage. However, the concrete produced a lot of damage, the energy dissipation increased significantly, and the stiffness decreased, which further proves that “the performance goal of the bottom frame structure is higher than that of the upper shear wall structure”.

## 6. Conclusions

1. The structural safety performance meets the seismic requirements of the MCE.
2. Under the action of load, the structure forms a reasonable damage mechanism that the members above the transfer story crack first and those below the transfer story crack later.
3. The transfer plate is mainly subject to shear deformation, the transfer plate will form shear failure, which should be avoided through reasonable design.
4. Because of the huge height difference between the first story and the second story (the subway on the first story), the structure may be adversely affected, so it is necessary to make the yielding floor appear in the bottom strengthening part above the transfer story through reasonable design.
5. Under the SLE and DBE conditions, the bottom frame of the structure is mainly subjected to elastic deformation. Under the MCE condition, the bottom frame of the structure produces a lot of damage, consumed energy increases, and stiffness decreases. The load capacity did not decline, which proves that “the performance goal of the bottom frame structure is higher than that of the upper shear wall structure”.

**Author Contributions:** Writing—original draft preparation, Y.X.; funding acquisition, W.L. (Wuxiong Li) and W.L. (Weiya Liu); Project administration, W.L. (Wuxiong Li) and W.L. (Weiya Liu); Supervision, Y.L.; Data curation, X.X.; Visualization, C.Z. All authors have read and agreed to the published version of the manuscript.

**Funding:** This work was mainly funded by the National Key R&D Project of China (No. 2021YFE0112200) and Natural Science Foundation of Guangdong Province (No. 2021A1515010586). Their support is gratefully acknowledged.

**Data Availability Statement:** Data are available with the first author and can be shared with anyone upon reasonable request.

**Conflicts of Interest:** The authors declare no conflict of interest.

## References

1. Li, J.H.; Su, R.; Chandler, A.M. Assessment of low-rise building with transfer beam under seismic forces. *Eng. Struct.* **2003**, *25*, 1537–1549. [[CrossRef](#)]
2. Zhou, X.; Xu, Y.L. Multi-hazard performance assessment of a transfer-plate high-rise building. *Earthq. Eng. Eng. Vib.* **2007**, *6*, 371–382. [[CrossRef](#)]
3. Su, R.; Chandler, A.; Li, J.; Lam, N. Seismic assessment of transfer plate high rise buildings. *Struct. Eng. Mech.* **2002**, *14*, 287. [[CrossRef](#)]
4. Kang, S.-M.; Na, S.-J.; Hwang, H.-J.; Kim, S.-I. Punching shear strength improved by upward panel in reinforced concrete transfer slabs. *J. Build. Eng.* **2022**, *46*, 103753. [[CrossRef](#)]
5. Kang, S.M.; Na, S.J.; Hwang, H.J. Two-way shear strength of reinforced concrete transfer slab-column connections. *Eng. Struct.* **2021**, *231*, 111693. [[CrossRef](#)]
6. Kang, S.M.; Na, S.J.; Hwang, H.J. Punching shear strength of reinforced concrete transfer slab-column connections with shear reinforcement. *Eng. Struct.* **2021**, *243*, 112610. [[CrossRef](#)]
7. Lee, H.S.; Ko, D.W. Seismic Response Characteristics of High-Rise RC Wall Buildings Having Different Irregularities in Lower Stories. *Steel Constr.* **2007**, *29*, 3149–3167.
8. Wang, W.; Chen, Y.; Dong, B.; Leon, R.T. Experimental behavior of transfer story connections for high-rise SRC structures under seismic loading. *Earthq. Eng. Struct. Dyn.* **2010**, *40*, 961–975. [[CrossRef](#)]
9. Wu, Y.; Nong, X. Research and application of high-rise building structural system on upper part of metro depot. *Build. Struct.* **2020**, *50*, 90–95. [[CrossRef](#)]
10. Moehle, J.P. Seismic Response of Vertically Irregular Structures. *J. Struct. Eng.* **2014**, *110*, 2002–2014. [[CrossRef](#)]
11. Yoshimura, M. Nonlinear analysis of a reinforced concrete building with a soft first story collapsed by the 1995 Hyogoken-Nanbu earthquake. *Cem. Concr. Compos.* **1997**, *19*, 213–221. [[CrossRef](#)]
12. Beigi, H.A.; Sullivan, T.J.; Christopoulos, C.; Calvi, G.M. Factors influencing the repair costs of soft-story RC frame buildings and implications for their seismic retrofit. *Eng. Struct.* **2015**, *101*, 233–245. [[CrossRef](#)]
13. Benavent-Climent, A.; Mota-Páez, S. Earthquake retrofitting of R/C frames with soft first story using hysteretic dampers: Energy-based design method and evaluation. *Eng. Struct.* **2017**, *137*, 19–32. [[CrossRef](#)]

14. Mazza, F.; Mazza, M.; Vulcano, A. Base-isolation systems for the seismic retrofitting of r.c. framed buildings with soft-storey subjected to near-fault earthquakes. *Soil Dyn. Earthq. Eng.* **2018**, *109*, 209–221. [[CrossRef](#)]
15. Giannakouras, P.; Zeris, C. Seismic performance of irregular RC frames designed according to the DDBD approach. *Eng. Struct.* **2019**, *182*, 427–445. [[CrossRef](#)]
16. Javadi, P.; Yamakawa, T. Strength and ductility type retrofit of soft-first-story RC frames through the steel-jacketed non-reinforced thick hybrid wall. *Eng. Struct.* **2019**, *186*, 255–269. [[CrossRef](#)]
17. Jara, J.M.; Hernández, E.; Olmos, B.A.; Martínez, G. Building damages during the September 19, 2017 earthquake in Mexico City and seismic retrofitting of existing first soft-story buildings—ScienceDirect. *Eng. Struct.* **2020**, *209*, 109977. [[CrossRef](#)]
18. Mouhine, M.; Hilali, E. Seismic vulnerability assessment of RC buildings with setback irregularity—ScienceDirect. *Ain Shams Eng. J.* **2021**, *13*, 101486. [[CrossRef](#)]
19. Pm, A.; Gpk, B. Reinforced concrete setback frame structure: A seismic analysis—ScienceDirect. *Mater. Today Proc.* **2021**. *Withdrawn Article in Press.* [[CrossRef](#)]
20. Nasab, M.; Chun, S.; Kim, J. Soil-structure interaction effect on seismic retrofit of a soft first-story structure. *Structures* **2021**, *32*, 1553–1564. [[CrossRef](#)]
21. Hareen, C.; Mohan, S.C. Evaluation of seismic torsional response of ductile RC buildings with soft first story. *Structures* **2021**, *29*, 1640–1654. [[CrossRef](#)]
22. Jiang, H.; Huang, Y.; He, L.; Huang, T.; Zhang, S. Seismic performance of RC frame-shear wall structures with vertical setback. *Structures* **2021**, *33*, 4203–4217. [[CrossRef](#)]
23. Sarkar, P.; Prasad, A.M.; Menon, D. Vertical geometric irregularity in stepped building frames. *Eng. Struct.* **2010**, *32*, 2175–2182. [[CrossRef](#)]
24. Lin, J.L.; Tsaur, C.C.; Tsai, K.C. Two-degree-of-freedom modal response history analysis of buildings with specific vertical irregularities. *Eng. Struct.* **2019**, *184*, 505–523. [[CrossRef](#)]
25. Stefano, M.D.; Pintucchi, B. A review of research on seismic behaviour of irregular building structures since 2002. *Bull. Earthq. Eng.* **2008**, *6*, 285–308. [[CrossRef](#)]
26. Sahoo, D.R.; Rai, D.C. Design and evaluation of seismic strengthening techniques for reinforced concrete frames with soft ground story. *Eng. Struct.* **2013**, *56*, 1933–1944. [[CrossRef](#)]
27. Pavel, F.; Carale, G. Seismic assessment for typical soft-storey reinforced concrete structures in Bucharest, Romania. *Int. J. Disaster Risk Reduct.* **2019**, *41*, 101332. [[CrossRef](#)]
28. Eom, T.S.; Song, J.W.; Song, J.K.; Kang, G.S.; Yoon, J.K.; Kang, S.M. Punching-shear behavior of slabs with bar truss shear reinforcement on rectangular columns. *Eng. Struct.* **2017**, *134*, 390–399. [[CrossRef](#)]
29. Sahoo, S.; Singh, B. Punching shear capacity of recycled-aggregate concrete slab-column connections. *J. Build. Eng.* **2021**, *41*, 102430. [[CrossRef](#)]
30. Yuan, B.; Chen, W.; Zhao, J.; Li, L.; Liu, F.; Guo, Y.; Zhang, B. Addition of alkaline solutions and fibers for the reinforcement of kaolinite-containing granite residual soil. *Appl. Clay Sci.* **2022**, *228*, 106644. [[CrossRef](#)]
31. Park, H.G.; Choi, K.K. Strength of exterior slab-column connections subjected to unbalanced moments. *Eng. Struct.* **2007**, *29*, 1096–1114. [[CrossRef](#)]
32. Zhang, X.; Wu, Y.; Zhai, E.; Ye, P. Coupling analysis of the heat-water dynamics and frozen depth in a seasonally frozen zone. *J. Hydrol.* **2021**, *593*, 125603. [[CrossRef](#)]
33. Zhang, X.; Zhai, E.; Wu, Y.; Sun, D.; Lu, Y. Theoretical and Numerical Analyses on Hydro-Thermal-Salt-Mechanical Interaction of Unsaturated Salinized Soil Subjected to Typical Unidirectional Freezing Process. *Int. J. Geomech.* **2021**, *21*, 04021104. [[CrossRef](#)]
34. Truong, G.T.; Choi, K.K.; Kim, C.S. Punching shear strength of interior concrete slab-column connections reinforced with FRP flexural and shear reinforcement. *J. Build. Eng.* **2021**, *46*, 103692. [[CrossRef](#)]
35. El-Gendy, M.; El-Salakawy, E. Effect of flexural reinforcement type and ratio on the punching behavior of RC slab-column edge connections subjected to reversed-cyclic lateral loads. *Eng. Struct.* **2019**, *200*, 109703. [[CrossRef](#)]
36. Kai, Q.; Jsl, A.; Th, B.; Yhw, A.; Xfd, B. Punching shear strength of corroded reinforced concrete slab-column connections. *J. Build. Eng.* **2021**, *45*, 103489.
37. GB 50011-2010; Chinese Ministry of Housing and Urban-Rural Development, Code for Seismic Design of Buildings. China Architecture and Building Press: Beijing, China, 2010.
38. DBJ/T 15-151-2019; Guangdong Provincial Department of Housing and Urban-Rural Development, Specification for Performance-Based Seismic Design of Reinforced Concrete Building Structure. China City Press: Beijing, China, 2019.